Identifying Fragilities in Biochemical Networks: Robust Performance Analysis of Fas Signaling-Induced Apoptosis

Jason E. Shoemaker* and Francis J. Doyle III*†
*Department of Chemical Engineering and †Department of Biomolecular Science and Engineering, University of California, Santa Barbara, California

ABSTRACT Proper control of apoptotic signaling is critical to immune response and development in multicellular organisms. Two tools from control engineering are applied to a mathematical model of Fas ligand signaling-induced apoptosis. Structured singular value analysis determines the volume in parameter space within which the system parameters may exist and still maintain efficacious signaling, but is limited to linear behaviors. Sensitivity analysis can be applied to nonlinear systems but is difficult to relate to performance criteria. Thus, structured singular value analysis is used to quantify performance during apoptosis rejection, ensuring that the system remains sensitive but not overly so to apoptotic stimuli. Sensitivity analysis is applied when the system has switched to the death-inducing, apoptotic steady state to determine parameters significant to maintaining the bistability. The analyses reveal that the magnitude of the death signal is fragile to perturbations in degradation parameters (failures in the ubiquitin/proteasome mechanism) while the timing of signal expression can be tuned by manipulating local parameters. Simultaneous parameter uncertainty highlights apoptotic fragility to disturbances in the ubiquitin/proteasome system. Sensitivity analysis reveals that the robust signaling characteristics of the apoptotic network is due to network architecture, and the apoptotic signaling threshold is best manipulated by interactions upstream of the apoptosome.

INTRODUCTION

Drug therapies seek to manipulate cellular processes to promote specific phenotypic outcomes. In many cases, such as inoculations, the drug seeks to enhance the health of the cellular population (1), but in cases such as cancer eradication, therapy ultimately seeks to destroy the cell (2). Future drug development will employ multitargeted procedures so as to manipulate specific intracellular processes without compromising critical, auxiliary processes, and thus reducing unnecessary side affects (3,4). To aid in target identification, mathematical models of biological processes such as cellular signaling, apoptosis, metabolism, etc. are being developed to relate perturbations (either in protein concentration, transcriptional activity, etc.) to their ensuing consequences on cellular performance and health. In this work, a model of Fas signaling-induced apoptosis, a form of cellular suicide crucial to immune response, is analyzed for robust performance. The ensuing fragilities revealed in the network identifies network components whose manipulation best controls the apoptotic response.

Robust performance is the ability to maintain desired performance specifications regardless of disturbances or uncertainties. Complex systems operating in real world scenarios must be robust to the uncertainties manifested in their environments and within themselves. Biological systems function robustly despite uncertainty due to stochastic phenomena (5), fluctuating environments, and genetic variation (see (6) for a review on robustness in cellular systems), and, therefore, demand great amounts of regulation to protect critical elements. To cope with uncertain intra- and extracellular conditions, biology has opted to use feedback, redundancy, and modularity strategies to protect critical network components (7). Fragility is the antithesis of robustness. Generally speaking, specific network behaviors may be robust to particular uncertainties and perturbations but heavily modulated by interactions to which the network is fragile. By understanding the robust elements of cellular signaling mechanisms and identifying their fragilities, it may be possible to manipulate cellular networks so that side effects on other systems, invariably related due to the high levels of crosstalk in biology, are minimal.

Complex, multicellular organisms require the ability to safely and efficiently remove superfluous, damaged, and potentially malignant cells from the population without damaging neighboring cells. Apoptosis is the intracellular, suicide program designated to the removal of byproduct cells produced during development (8) and responsible for the elimination of cells targeted by immune response (9). The death signal resulting in apoptosis can originate either internally, as in the case of DNA-damage, or externally when activated T lymphocytes bind their target cells (10). The severity of the output from the apoptotic program demands tight regulation of the death signal, and failure to accurately process apoptotic signaling has been implicated in the pathogenesis of several forms of cancer (11). As such, several layers of often redundant regulation exist to ensure accurate processing of the death signal. Mathematical models that attempt to capture the dynamics of apoptotic signaling generally cluster several layers of interactions into a single parameter, thus giving rise to highly variable parameter sets.

Several methods have been applied to biological systems to quantify cellular network robustness. Monte Carlo type

Submitted October 10, 2007, and accepted for publication April 22, 2008.

Address reprint requests to Francis J. Doyle, Tel.: 805-893-8133; E-mail: doyle@engineering.ucsb.edu.

Editor: Costas D. Maranas.

0006-3495/08/09/2610/14 $2.00

doi: 10.1529/biophysj.107.123398

algorithms and brute force simulation was applied to bacterial chemotaxis to verify that the precision of adaptation is robust to parameter uncertainty but adaptation time is sensitive (12). Sensitivity has been applied to circadian rhythm models, concluding that circadian systems are often more fragile to perturbations in global parameters (transcriptional and translational machinery) than local parameters, a characteristic which appears to be the result of network topology as opposed to parameter tuning (13,14). Specific to apoptosis, simplified models which allow for bistability and ultrasensitive signaling have been analyzed via bifurcation analysis to measure the bistable parameter subspace for a selected subset of parameters (15). The tool of choice for quantifying network robustness in engineering is the structured singular value, as the results are less sensitive to the discretization of parameter space (as in the case of Monte Carlo/brute force techniques), results can be directly attributed to specified performance criteria (often difficult in sensitivity analysis), and the analysis is not limited by visualization constraints (bifurcation analysis). Margin analysis (a one-dimensional equivalent of structured singular value (SSV) analysis) was employed by Schmidt and Jacobsen (16) for model reduction and identification of key interactions maintaining intracellular dynamic behaviors such as circadian and cell cycle oscillations.

To identify the robust components of the Fas signaling-induced apoptosis system, a mathematical model is analyzed using structured singular values (SSVs) and sensitivity analysis. SSV analysis determines whether a dynamical system can maintain defined performance attributes for a given (structured) set of uncertainties. Sensitivity analysis measures the degree with which the apoptotic system's trajectory shifts, given infinitesimal perturbations in its parameter values. SSV analysis guarantees that the system maintains performance for all permutations of parameter values defined in the uncertain parameter space but is limited by nonlinearities in the system. Though it may be applied to nonlinear systems, sensitivity analysis only considers infinitesimal perturbations. In the Fas apoptosis system, a linear approximation well characterizes the system dynamics when the system is exposed to a death signal below the threshold to induce apoptosis, but the quality of the approximation is severely diminished when the stability of the system switches to its upper/apoptotic steady state. Thus, SSV analysis is used to quantify apoptotic robustness during noise rejection, when the death signal is below the threshold, and sensitivity analysis is used to quantify system robustness to parameter uncertainty when the system evolves toward apoptosis.

THEORY

Sensitivity analysis

Sensitivity is the response of the state trajectory to an infinitesimal disturbance in a nominal parameter value (17), and, in this work, the sensitivity is normalized by both parameter and state sizes to yield a relative measure. For a lumped system model given by $\dot{x} = f(x,p)$, the relative sensitivity is defined to be

$$\hat{S} = \frac{\partial x}{\partial p} \times \frac{p}{x} = \frac{\partial \ln(x)}{\partial \ln(p)}, \tag{1}$$

where x is the state vector(protein concentrations, expression levels, etc.) and p is a parameter vector. Sensitivity analysis has been used in several fields to guide model reduction (18), and to explore robustness phenomena in biochemical systems (14,19). The BioSens Toolkit (20) is employed to calculate the sensitivity over varying parameter sets so as to approximate a semiglobal understanding of the system's behavioral dependence on parameter fluctuations.

Structured singular values

The structured singular value (SSV) is used to analyze the properties of stability and performance in a system for a given, bounded set of internally or externally occurring uncertainties. A system that maintains stability for all feasible disturbances is said to have the property of robust stability (RS). A system has the property of robust performance (RP) if its input/output response can be bounded within operational ranges despite system uncertainties. SSV analysis is a well-studied tool for robustness analysis in engineering, and software packages are available (21). SSV analysis has been used to explore robust performance characteristics of a variety of engineering systems from chemical processes (22) to flight control (23). The first step to SSV analysis is to formulate, via linear fractional transformations, the system into the $N\Delta$ block structure (see Fig. 1), describing all system uncertainties into a normalized, block-diagonal $\mathbf{\Delta}$ such that the maximum singular value of $\mathbf{\Delta}$, $\overline{\sigma}(\mathbf{\Delta})$, is ≤ 1. Applying Nyquist stability criterion, we are guaranteed robust stability of the original uncertain system so long as the destabilizing $\mathbf{\Delta}$, calculated via Nyquist criterion, maintains the condition of $\overline{\sigma}(\mathbf{\Delta}) \geq 1$. The value of μ is formally defined as

$$\mu(\mathbf{M})^{-1} \triangleq \min_{\Delta} \{\overline{\sigma}(\Delta) | \det(\mathbf{I} - \mathbf{M}\Delta) = \mathbf{0} \text{ for structured } \Delta\}. \tag{2}$$

Thus, $\mu > 1$ implies $\overline{\sigma}(\mathbf{\Delta}) \leq 1$, and some combination of parameter values within the uncertain parameter space allows the system to be unstable. The calculation of μ is an NP-hard problem, and the interested reader is referred to the original citations for more details (24,25). For 2×2 input/output systems, exact solutions exist, but for larger systems, lower and upper bounds on μ are calculated. Appendix B provides more background information.

Robust performance can be tested in a similar fashion. By closing the input/output channels of the $N\Delta$ block, one can guarantee robust performance on the uncertain system by

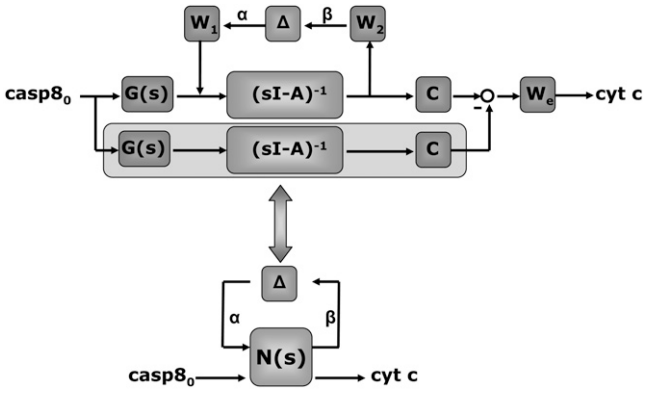

FIGURE 1 Block diagram of the linear system. The nonlinear system is linearized about the nonapoptotic steady state where A is the system Jacobian and C is a constant matrix stipulating cyt c as the output. $G(s)$ is created such that a step in the initial concentration of casp8 matches the dynamics of the nonlinear system when the concentration of casp8 is elevated to levels below the induction threshold. The uncertain system is created using constant matrixes $\mathbf{W}_1$ and $\mathbf{W}_2$ to distribute the uncertainties about the Jacobian. The difference between the responses of the nominal system (*highlighted*) and the uncertain system is weighted by the error filter ($\mathbf{W}_e$) such that, at frequencies when the response is most sensitive, the frequency gain can double or half its nominal response and maintain performance. This difference system is lifted to the $N\Delta$ block configuration and tested for robust performance.

testing for robust stability of the new, closed-loop circuit. For RS, the value of μ provides a stability margin in that multiplying the uncertainty block, Δ, by the inverse of μ will shift one stable eigenvalue to the imaginary axis. But doing so during RP will inadvertently effect the performance specifications. Thus, to address relationships between maximum performance for a given perturbation set, or vice versa, the largest allowable perturbation set for a given performance specification, a process of skewed-μ is employed in which the weightings of the individual perturbations are adjusted until $\mu = 1$ (26). For clarity throughout the text, SSV will be used in place of the variable μ, to avoid confusion with other conventions in biophysical modeling.

It should be noted that SSV analysis is a frequency-based analysis and care must be taken when drawing conclusions in the time domain based on dynamics observed in the frequency domain. The advantage of frequency-based analysis over stepwise perturbations or pulse analyses is that frequency analysis considers the system behavior to be a general class of input perturbations whose magnitude may be bounded.

METHODS

Type II, Fas ligand (FasL) signaling-induced apoptosis

The immune response targets the Fas signaling-induced apoptotic pathway during the destruction and removal of potentially pathogenic cells. Natural killer cells, macrophages, and activated T lymphocytes express Fas ligand (FasL) on their surfaces (9,10), and upon contacting their target cells, FasL binds to its receptor, initiating the death signal, and resulting in the activation of caspase 8 (casp8) (see Fig. 2). Fas is a member of the tumor necrosis factor superfamily, and is considered a key target for cancer therapy (27).

The death signal is amplified via the cleaving of Bid and the release of cytochrome c (cyt c) from the mitochondria. Cytosolic cyt c binds Apaf-1, forming the apoptosome. The apoptosome catalyzes procaspase 9's (pro9) transition to caspase 9, and caspase 9 catalyzes the production of the executioner caspase, caspase 3. Several models exist to explain and predict apoptotic network behavior (28–31). The model developed by Bagci et al. (32) consists of 31 ordinary differential equations and 65 parameters. Most interactions are simple, first-order mass action kinetics. A cooperative mechanism is assumed during apoptosome formation to account for the bistability observed in the Fas apoptotic system (33), a characteristic not universally observed in previous models. The argument for bistability in the caspase 3 concentration versus ultrasensitivity-type behavior is experimentally supported by Bentele et al. (28), in which the transition between two stable states was observed. Care is taken to preserve the nomenclature employed by Bagci et al. (32). Parameters with a μ or a G preceding a species name denote degradation and production terms. Throughout the analysis, the coefficient of Hill kinetics is considered to be part of network topology and not prone to uncertainty.

Linearization

The Fas signaling-induced apoptosis system is bistable, and therefore, linearized about both the (apoptotic) activated and (nonapoptotic) inactivated steady states. Both linearizations are compared against the dynamics of the nonlinear system (see Fig. 3). When a stimulus below the apoptosis-inducing threshold is introduced (initial casp8 concentration $<1 \times 10^{-4}$ μM), the linear approximation well characterizes the behavior of the original system, but the linear approximation is poorly suited for characterizing the behavior about the activated steady state.

Robust performance analysis during noise rejection

Selecting the nonapoptotic steady state to quantify the robustness of low signal input/noise rejection performance, the system is arranged into the block diagram seen in Fig. 1. The output of the system is cytosolic cyt c and the input is the initial concentration of casp8. Parameters are assigned a multiplicative uncertainty in the form of $\hat{k}_i = k_i(1+\delta_i * w_i)$ such that $\delta_i \in [-1\ 1]$ and w_i weights the perturbation. Parameter uncertainties are collected into the $\mathbf{\Delta}$ block, and $\mathbf{W_1}$ and $\mathbf{W_2}$ serve to both weight and distribute the uncertainties about the Jacobian ($\mathbf{A}$ block). To create the weighting blocks, the matrix $\hat{\mathrm{A}}$ is calculated from the Jacobian in which only entries pertaining to the parameters of interest are retained, all other entries are set to zero. The singular value decomposition of $\hat{\mathrm{A}}$ is taken as $\mathrm{SVD}(\hat{\mathrm{A}}) = \mathbf{U\Sigma V^H}$. Keeping only the nonzero components of $\mathbf{\Sigma}$ and the corresponding rows and columns of $\mathbf{U}$ and $\mathbf{V}$, $\mathbf{W_1}$ is set equal to $\mathbf{U} \times \mathrm{w_i}$ while $\mathbf{W_2}$ is set equal to $\mathbf{\Sigma V^H} \times \mathrm{w_i}$, where the w_i tunes the range parameter and k_i may vary. This procedure minimizes the rank of Δ for each uncertain parameter, but care must be taken when applying to multiple, simultaneous uncertain parameters so that coupling effects are not negated. The weighted transfer function, $G(s)$, is designed such that a step in casp8 has the equivalent effect on the system raising the initial concentration of casp8 to 1×10^{-5} μM.

The performance of the uncertain system is measured against the response of the nominal system. The difference between the two responses is weighted by $\mathbf{W_e}$, an error filter of the form

$$\mathbf{W_e} = \frac{(s + 03e - 3)^2}{6.2e - 6 \times (s + 1e - 4)}. \quad (3)$$

This error filter allows for approximately a halving or doubling of peak cyt c production, and an ~5 min gain/delay in cyt c signaling (limits computationally determined). Having set the performance criteria, skewed-μ is applied

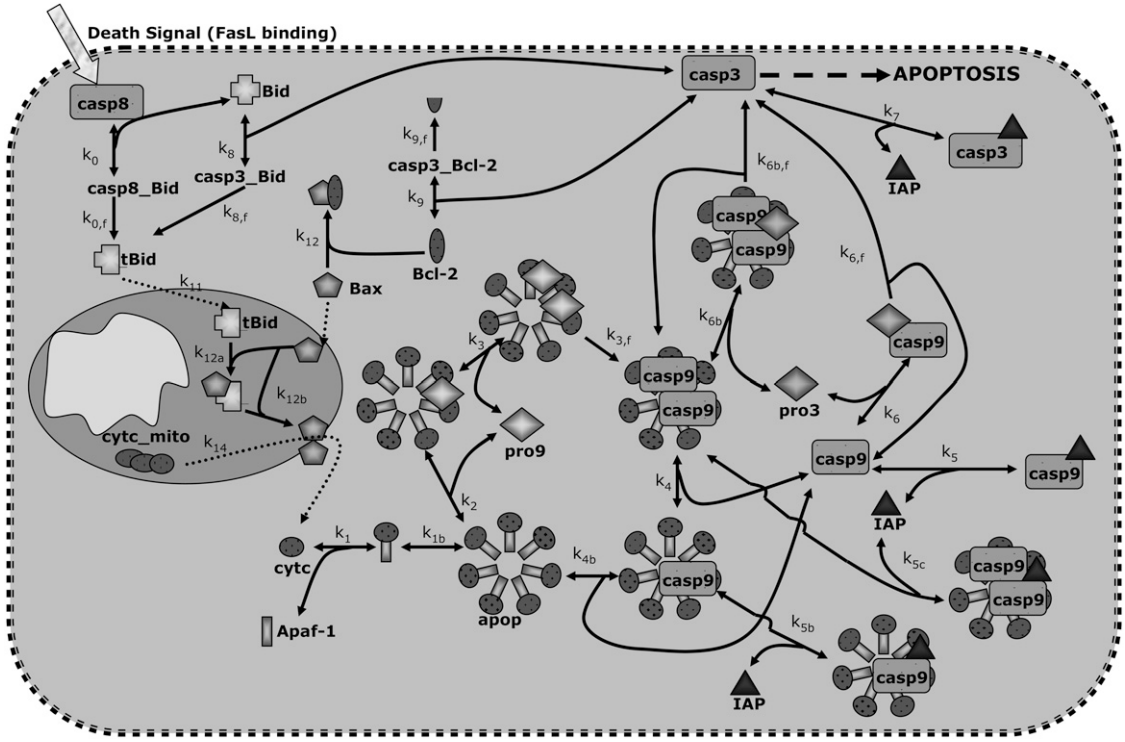

FIGURE 2 The signaling pathway of Type II, FasL signaling-induced apoptosis, adapted from Bagci et al. (32). Broken arrows represent translocation reactions. Double-headed arrows represent reversible reactions with forward and reversible reactions labeled as k_{ip} and k_{im}, respectively, throughout the text. Degradation and production parameters are denoted with a μ and a G, respectively, preceding the species label throughout the text.

to determine the maximum allowable parameter variation permitted before performance is lost. The allowable variation (AV) for parameter k_i is defined as $AV_i = \delta_i \times w_i \times 100$. It should be noted that production parameters do not appear in the Jacobian, and, therefore, cannot be analyzed by SSV analysis.

Sensitivity analysis during apoptotic expression

As the linear approximation about the apoptotic steady state poorly captures the dynamics of the nonlinear response, sensitivity analysis is used to identify the parameters which most affect the system during evolution to apoptosis. Only the sensitivity of casp3 is considered. To develop a semiglobal understanding of parameter fluctuation on the apoptotic response, casp3 sensitivity is calculated for 500 parameter sets. Each parameter set is generated by applying a Monte Carlo algorithm, randomly perturbing elements of the nominal parameter set up to $\pm 5.0\%$. Each of the 500 parameter sets are tested for an apoptotic response to 1×10^{-4} μM casp8. The normalized sensitivity for those sets which induce apoptosis is calculated for 10,000 s. The absolute values of the normalized sensitivities are then summed over time.

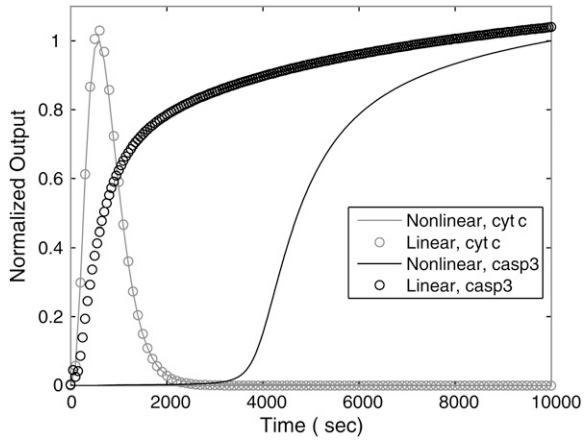

FIGURE 3 Comparing the linear and nonlinear models to casp8 below (1×10^{-5} μM) and above (1×10^{-4} μM) the threshold concentration. The output for the models linearized about the nonapoptotic and apoptotic steady states are cyt c and casp3, respectively. The linear outputs are mapped in circles and the nonlinear outputs are solid lines.

RESULTS

During noise rejection, performance limited by cyt *c* leakage, Bid cleavage

Procasp8 (the inactive form of casp8) is ubiquitously expressed in cells, and cells must be robust to mild perturbations in the concentration of casp8. Linearization about the nonapoptotic steady state reveals that only network components upstream of the apoptosome formation are responsible for maintaining resistance to signal noise in the apoptotic network (elements downstream of cyt c leakage have a null transfer function). Bagci et al. (32) demonstrated that caspase 3 bistability is maintained primarily by the Hill kinetic description, and thus a reasonable performance specification is to bind the cyt c response to the apoptosome. Therefore, the performance specifications are chosen such that the cyt c nominal response is bounded above and below by a factor of one-half. The upper bound guarantees the cellular response is

not overly sensitive to intracellular fluctuations while the lower bound prevents a null apoptotic response to death signaling.

In Fig. 4, perturbing each parameter individually reveals that the performance of the death signal is most fragile (least robust) to variations in degradation machinery, cyt *c* leakage from the mitochondrial matrix into the cytosol (k_{12a}, k_{12b}, and k_{14}), and Bid/casp8 dissociation (k_{0m}, k_{0p}, and k_{0f}). All parameters not shown have an AV exceeding 100%, and the AV of their robust performance equals that of their robust stability, meaning instability is induced before performance failure.

Local interactions dictate timescales of death signal

In previous works, parameter were segregated, based on the distribution of their regulatory processes, into local, global, and mixed. Local parameters are interactions whose regulation is confined to the apoptotic network; global parameters are characterized by heavily regulated, core intracellular processes (translation, transcription, etc.); and mixed parameters are a union of the two (for a detailed discussion, see (14)). Interestingly, differing, fragile characteristics of the apoptotic signal can be exploited along these groupings. Of the 12 parameters shown in Fig. 4, degradation reactions are labeled global, as the proteasome is known to either directly or indirectly target the caspases (34), BLC-2, BAX (35), and other apoptosis cascade components (36). The remaining seven parameters are labeled as local as they are not regulated by any of the core processes. This is not to say they are not regulated by exterior processes as several processes (p53, JAK/STAT1, etc.) are known to interact with apoptotic signaling (37–39), but these interactions are not correlated to cell regulatory processes.

The frequency response of the perturbed, local parameters shows that both the phase and magnitude of the death signal

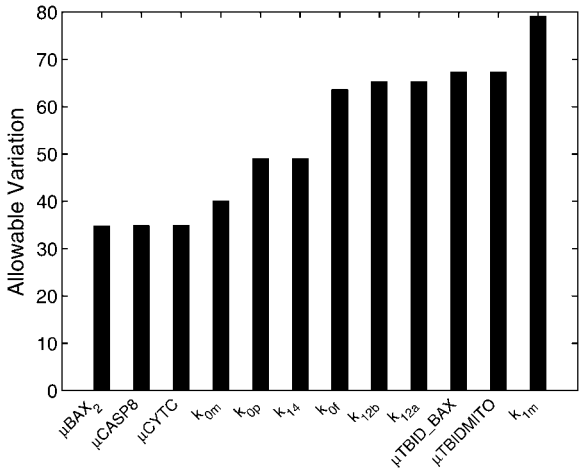

FIGURE 4 The allowable variation (AV) for the most sensitive parameters when perturbed individually. The AV is calculated by applying skewed-μ to determine the smallest perturbation which forces the system response to match performance limits. All parameters not shown have an AV $\geq$100%.

is fragile to uncertainty in the local set (see Fig. 5, *a* and *b*). Each parameter in the local subset is perturbed to by its AV, defined in Fig. 4, and its frequency response is plotted against the nominal response of the system. Perturbing the local parameters shifts both the phase and magnitude of the cyt *c* response. Particularly, uncertainty in the dissociation of Apaf-1 and cyt *c* (k_{1m}) strongly affects the timescales of apoptotic signaling, clearly visible in its phase response. To verify these fragile behaviors in the nonlinear system, the peak difference and the time shift of the peak expression of cyt *c* response in the full apoptotic model is measured while each parameter is perturbed by the fraction δ (i.e., $\hat{k}_i = k_i(1+\delta)$). Fig. 6, *a* and *b*, illustrate how perturbing the local parameters is mildly shifting the peak cyt *c* concentration, but greatly influencing the advance/delay of the signal. The limits of the linear approximation are visible in the response of k_{1m}. Comparing the response when $\delta = -0.7$ and $\delta = -0.8$, there is an exponential jump in the signal delay.

Global interactions strongly affect signal magnitude

Uncertainty in the global subset affects the magnitude of the cyt *c* response (see Fig. 5, *c* and *d*). Again, each parameter is perturbed to its respective AV, and the frequency response of the perturbed system is compared against the nominal cyt *c* response. While perturbing the global parameters shifts the linear, cyt *c* response up (all RP failing perturbations in this case are negative), the phase of the uncertain responses never shifts from the nominal. Fig. 6 *c* emphasizes the point that, in the full apoptotic system, uncertainty in the most fragile, global parameters strongly affect the magnitude of the cyt *c* response (the timing of the response is unaltered; data not shown). Furthermore, comparing the magnitude of the peak differences between Fig. 6, *a* and *c*, the effect of perturbing the global parameters versus the local parameters is approximately an order-of-magnitude higher.

Robust performance during multiple, simultaneous uncertainties

To identify the minimum set of perturbations required to manipulate apoptotic response, each subgroup is perturbed simultaneously. To determine the maximum volume in parameter space, each subset may occupy and maintain robust signaling performance. The same signal performance metrics are applied, and an optimization routine is applied to determine the greatest volume in parameter space for which robust performance is met. The optimization routine calculates the sensitivity of μ by perturbing each parameter 1.0%, and then reducing the weighting of the parameter identified as ''most sensitive.''

The AV of both groupings is highly restricted when considering multiple parametric perturbations. Fig. 7 shows the maximum volume in parameter space for which performance is satisfied. For the global parameters, the shape of the subspace satisfying performance resembles that of the AV when

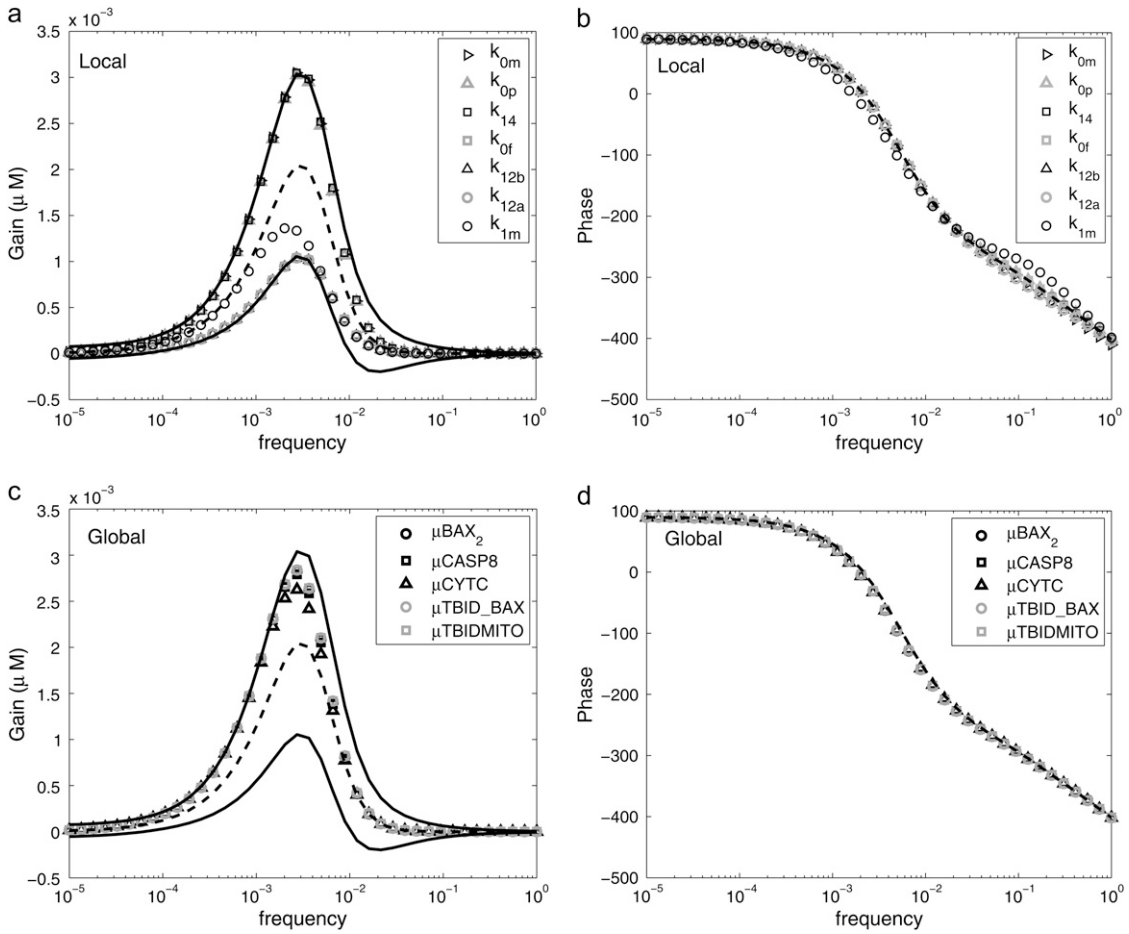

FIGURE 5 The gain and phase of the frequency response when the fragile parameters are perturbed to the limits of their allowable variations. Parameters are segregated into local (subplots *a* and *b*) and global (subplots *c* and *d*) subsets. The performance bounds are solid lines, and the nominal response is the dashed line.

parameters vary individually in isolation. The most restricted is the degradation of casp8 (8.3%) while the degradation of TBID_BAX can allow up to 14.4% uncertainty in its parameter value. For local parameters, the shape of the parameter subspace satisfying performance differs significantly from that of the subspace identified when allowing individual parameter perturbations. The AV of cyt *c*/Apaf-1 dissociation (k_{1m}) remains the most robust ($AV = 42.1\%$), while cyt *c* leakage (k_{14}) and casp8 cleavage of Bid (k_{0p}, k_{0m}, and k_{0f}) are severely restricted (between 6.25 and 7.11% AV). To identify which characteristic of the death signal is being modulated by these perturbations, the frequency response of the linearized system is calculated for the perturbation sets identified (see Fig. 7, *c* and *d*). Now, unlike the case where parameters are perturbed individually, simultaneous perturbations in both the global and local parameters amplify the magnitude of cyt *c* response, and the timescales of the response are unaffected.

As the dynamics of diffusion are poorly resolved in this model, the maximum parameter subspace which satisfies RP was calculated with the condition that cyt *c* leakage maintain an AV of 25.0%. As seen in Fig. 7, this additional constraint greatly restricts the volume of the uncertain subspace. Maintaining 25.0% AV in cyt *c* leakage (k_{14}) restricts the AV of all other fragile parameters to within 3.3–9.8% (k_{0m} and k_{1m}, respectively).

Both noise rejection and apoptotic expression are more sensitive to global parameters

Nonlinearities dominate the apoptotic response once casp8 has exceeded its threshold value; thus, sensitivity analysis is used to identify the significant interactions when the model follows apoptotic trajectories. A Monte Carlo algorithm is used to generate 500 parameter sets in which each parameter may be perturbed to within 5.0% of its nominal value. For each parameter set, the system is given an initial stimulus 1×10^{-4} μM casp8, then simulated to determine whether the parameter set allows for apoptosis. The parameter sets are segregated into two groups, apoptotic-inducing and non-apoptotic-inducing, and their sensitivities are calculated as discussed in the Theory section. The sensitivities are calculated with respect to casp3 production only.

For apoptotic and nonapoptotic parameter sets, the death signal is significantly more sensitive to perturbations in the

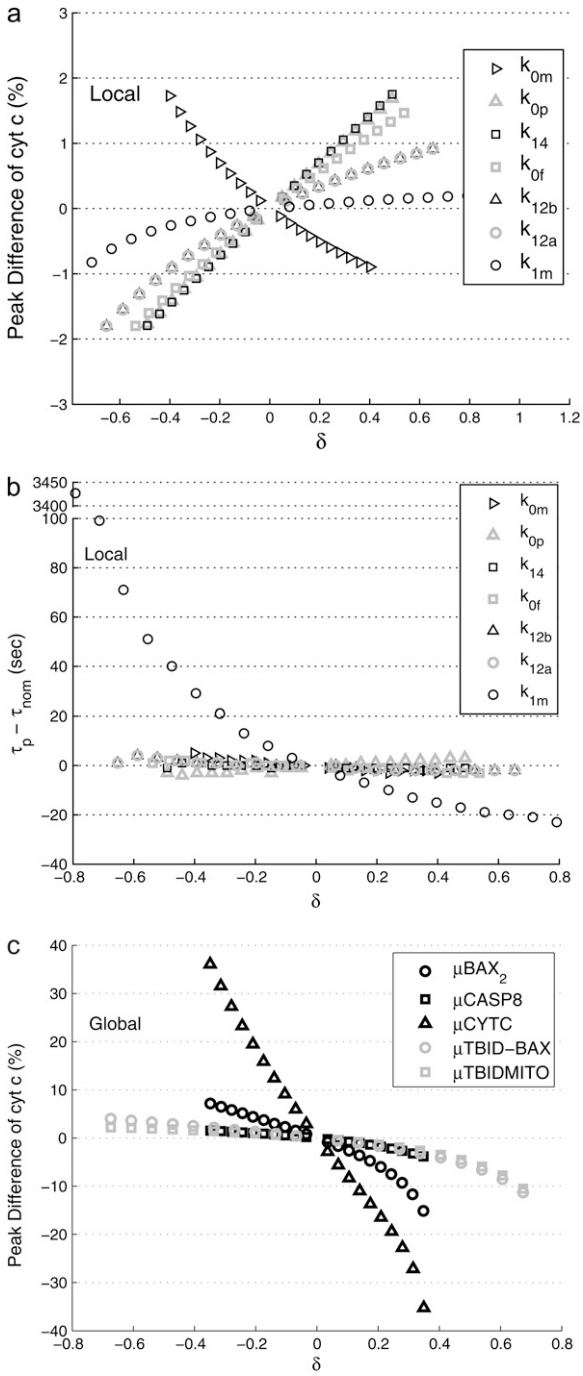

FIGURE 6 Comparison of the perturbed, nonlinear response to the nominal apoptotic system. Cyt *c* has a pulse response (see Fig. 3). Parameters are segregated into local (subplots *a* and *b*) and global (subplot *c*) subsets. Peak difference is the maximum value of the peak cyt *c* concentration of the nominal system subtracted from the perturbed response, reported in percentage change. The difference in τ_p (the time of expression of maximum cyt *c* concentration for the perturbed response) and τ_{nom} (the time of expression of maximum cyt *c* concentration in the nominal model) measures the delay of the death signal (negative values are signal advances). Expression timing data are not shown for global parameters, since the results are negligible. The value δ is the fraction each parameter is perturbed.

global parameters. Fig. 8 illustrates the normalized sensitivity distribution for the apoptotic and nonapoptotic scenarios. The apoptotic and nonapoptotic global subsets have log normal-like distributions while the local subsets appear bimodal on a log scale. The mean of the normalized sensitivity for the global parameters for the nonapoptotic and apoptotic cases (4.09×10^3 and 5.93×10^3, respectively) is significantly higher than their local counterparts (1.70×10^3 and 2.51×10^3, respectively). The distributions of the sensitivities of the global and local sets show distinct differences in how uncertainty within each subset effects apoptotic signaling. Global parameters are narrowly distributed while local parameters have trimodal distributions.

Sensitivity analysis during apoptotic response identifies the activation of casp3 via casp9 as fragile

The nonapoptotic-inducing subset supports the previous results, since the same interactions identified as fragile during SSV analysis of noise rejection are also identified as most sensitive (see Fig. 9). No restrictions are set on the shape of the casp3 time trajectory except that after 10,000 s, casp3 concentration is $<10^{-6}$ μM, but it is generally observed that casp3 decreases monotonically. The parameters are then ranked from 1 to 65, 1 being the most sensitive, and their respective standard deviations are shown. As observed during SSV analysis of noise rejection, sensitivity analysis identifies perturbations in degradation and production machinery (global variables) as most significant. As for local interactions, cyt *c* leakage due to Bid/Bax interaction during mitochondrial channel formation (k_{12a}, k_{12a}, and k_{14}), Bid cleavage via casp8, and Apaf-1/cyt *c* dimerization, are most sensitive. These results support assumptions made during SSV analysis in that regulation of the death signal during noise rejection is primarily dependent on intracellular machinery upstream of apoptosome formation. Thus, little was lost by the linearization and application of performance criteria to the cyt *c* response.

Many of the parameter rankings are preserved between the apoptotic- and nonapoptotic-inducing parameters sets. Apoptotic-producing sets are defined as parameter sets for which casp3 production has exceeded 1×10^{-4} μM after 10,000 s. Generally, apoptotic-inducing sets followed the same sigmoidal-shaped curve produced by the nominal set. No oscillations or other dynamic behaviors are observed. Comparing the parameters rankings of the apoptotic and the nonapoptotic parameter sets, no excessively major shifts in parameter rankings occur, but statistically significant variations within the top sensitive parameters are observed. The death signal is increasingly sensitive to the production of pro3 and pro9 (parameter numbers 3 and 4, respectively) as well as the degradation of pro9 (parameter number 13). Furthermore, pro3 activation via casp9 becomes a significant local, downstream interaction (parameter numbers

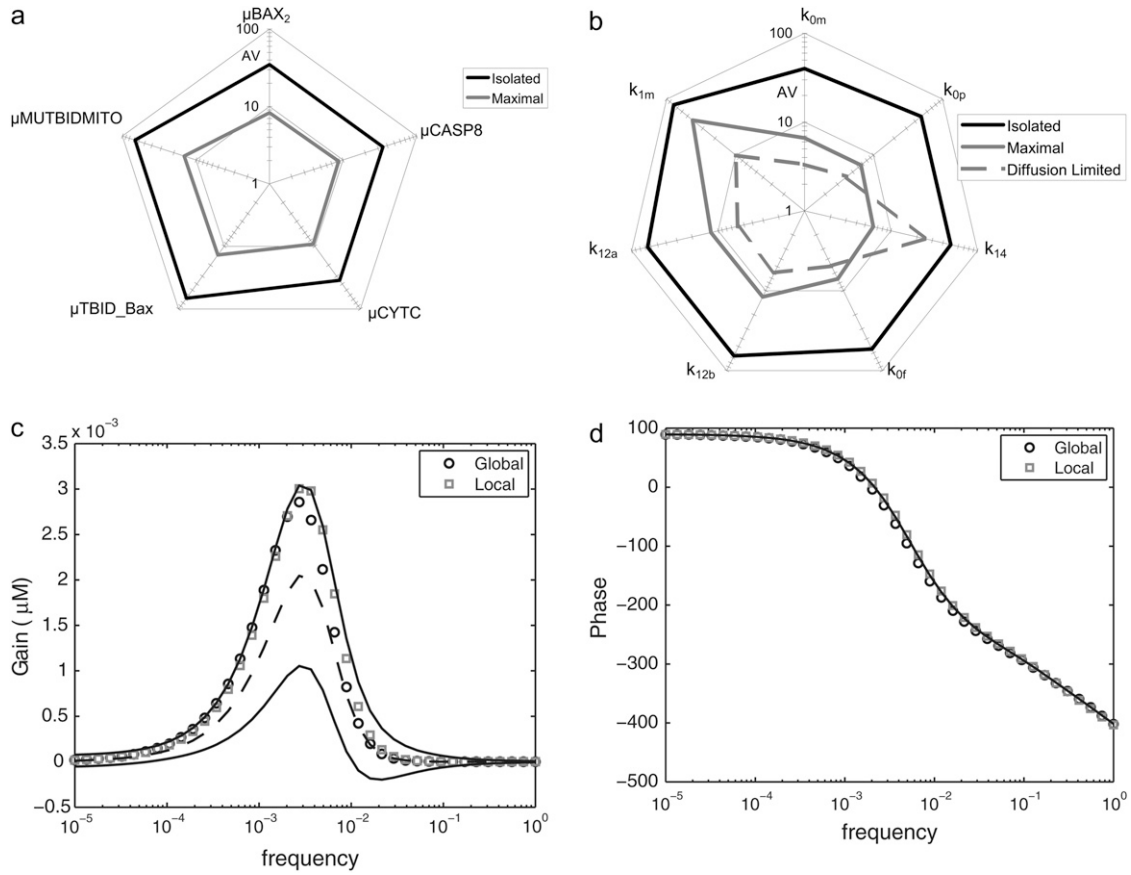

FIGURE 7 The AV when parameters can fluctuate simultaneously. Each parameter in the defined subsets (global *a* and local *b*) are allowed to vary simultaneously, and an optimization program employing skewed-μ is applied to determine the maximum volume in parameter space within which parameters can vary and maintain performance. For the local parameters, an additional calculation was performed to determine the largest parameter subspace for which performance is met with the additional constraint that diffusion (k_{14}) be allowed to vary $\pm$ 25% of its nominal value. The frequency response for the optimal AV for both the global and local parameter sets are panels *c* and *d*.

47–49). To test whether the observed variation of the sensitivity means is statistically valid, the *p*-values are calculated. Appendix A list all the parameters, their respective parameter numbers, rankings, and the *p*-value when comparing the distribution of their nonapoptotic and apoptotic sets.

Feedforward and feedback in apoptotic signaling insensitive to parameter uncertainty

The bistability of the apoptotic signaling network may be further maintained by the feedforward regulation via direct activation of casp3 by casp8 and feedback regulation via casp3 binding of Bcl-2. None of the parameters associated with these

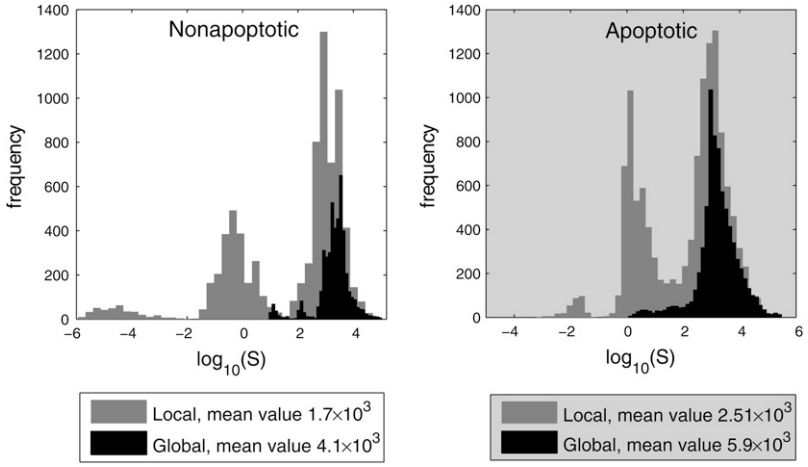

FIGURE 8 The distributions of the normalized sensitivity of casp3 for local and global parameter subsets. A Monte Carlo algorithm generates 500 parameters set by randomly perturbing the nominal parameter values $\pm$5.0%. Parameter sets for which a stimulus of 1×10^{-4} μM induces apoptosis are labeled apoptotic; otherwise they are labeled nonapoptotic.

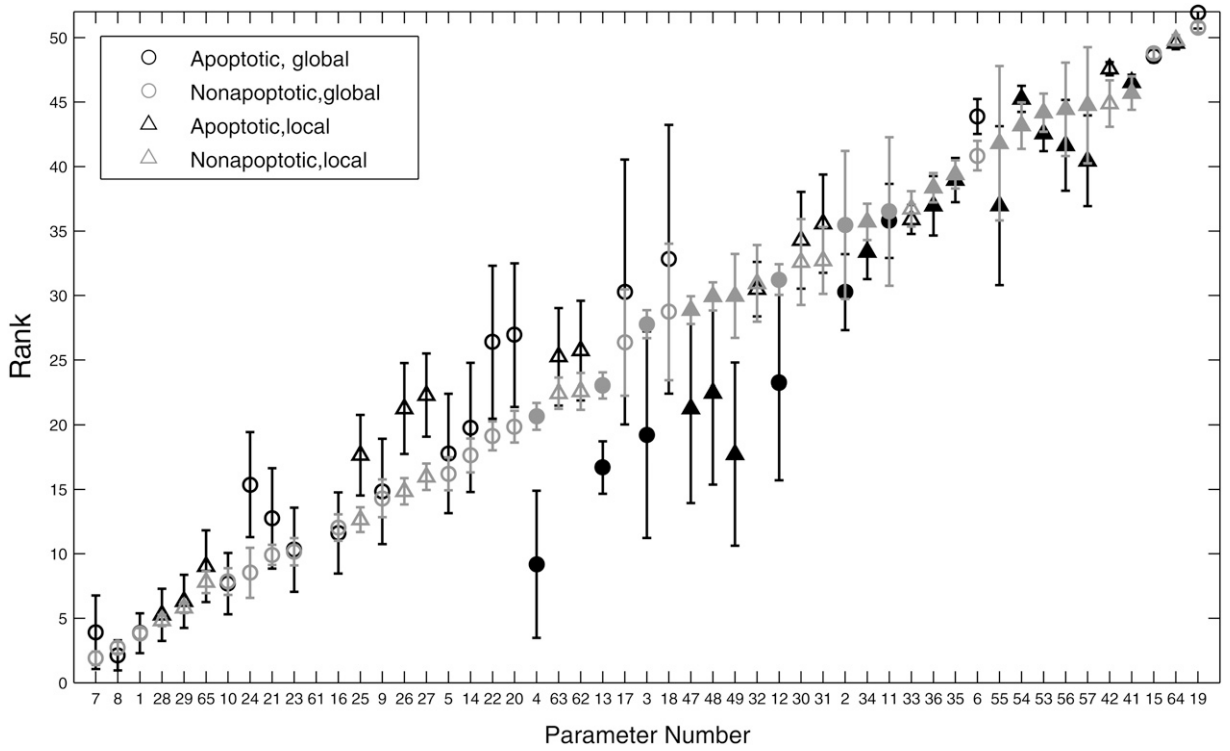

FIGURE 9 Mean parameter rankings and their respective standard deviations. A Monte Carlo algorithm is used to generate 500 parameter sets by randomly perturbing nominal parameter values up to 5.0%. Parameter sets are segregated into apoptotic (*solid*) and nonapoptotic (*shaded*) inducing sets (when a stimulus of 1×10^{-4} μM is applied). Each parameter is ranked according to the mean of its normalized sensitivity of casp3 over the generated parameter space. Parameters for which the mean sensitivity is statistically different when comparing the apoptotic versus nonapoptotic cases are indicated by solid circles (global) or solid triangles (local). All parameters and their respective parameter numbers are listed in the Appendix.

regulatory mechanisms appear in the top sensitive parameters, allowing for two hypotheses. It may be that these regulatory loops are not essential for bistable behavior; or they may be both necessary and robust to parameter perturbations. To test these hypotheses, the related parameters are set to zero and the bistable characteristics of the system are tested.

Removal of the feedback loop (k_{9p} and k_{9m} are set to zero) effects neither the existence of the bistability nor the threshold value (data not shown), whereas removal of the feedforward regulation (k_{8p} and k_{8m} are set to zero) eliminates the bistability. This feedforward structure is then perturbed to determine how fluctuations in the feedforward regulation affect the signaling threshold value. Fig. 10 illustrates how the apoptotic signaling threshold shifts as the strength of the feedforward regulation is knocked down. The value of the threshold stays nearly constant at $\sim 1 \times 10^{-4}$ μM initial casp8 until the feedforward is reduced by 80% ($\delta = 0.8$), then the threshold value rapidly rises until bistability is no longer feasible.

DISCUSSION

Understanding robustness in apoptosis and identifying network fragilities is crucial to designing therapies that align naturally occurring cellular machinery against malignant cell populations. Several works have focused on exploring modules of the apoptotic network, trying to identify canonical schemes which can ensure robust bistability while maintaining ultrasensitivity and induction characteristics (15,32,40). Here, robustness analyses is applied to the two distinct phases in apoptotic behavior as described by Nair et al. (33). The first, analyzed by SSV analysis, is a low-level input, noise rejection

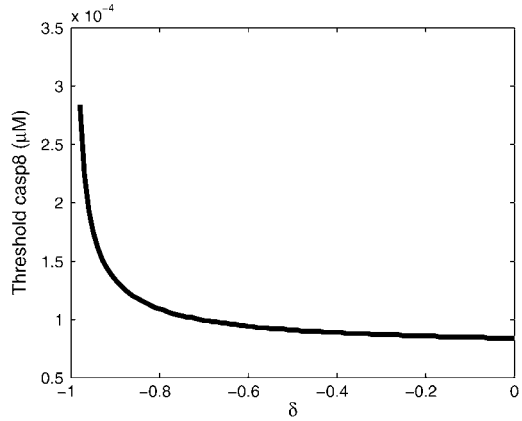

FIGURE 10 The threshold value of initial casp8 required to induce apoptosis is calculated while reducing the strength of the feedforward regulation. Multiplicative perturbations are applied to parameters k_{8m} and k_{8p}, and the value of initial casp8 is raised until apoptosis is achieved. Eliminating feedforward regulation ($\delta = -1$) eliminates bistability.

phase, when the apoptotic mechanism must filter out intracellular variation to prevent improper apoptotic expression. The second phase is the proper amplification and processing of the death signal once the initiating stimulant surpasses the necessary threshold.

Both analytical tools identify the same optimal set of interactions to manipulate apoptotic signaling during low level, noise stimulation, despite the application of robust performance criteria during SSV analysis. Sensitivity analysis is often applied to identify network fragilities, but the nature of these fragilities are often ambiguous. And while groups are working on developing specialized sensitivity analyses for specified behaviors (phase and gain sensitivity in circadian oscillators), in many cases, sensitivity analysis is applied without regard to the widely varying behaviors being generated in the system. Here, we have shown that calculating parameter sensitivity over several sets, and segregating the results based on loosely defined bistability criteria, the same parameter set identified when using a more powerful, semi-global technique can be regenerated. Thus, applied properly, sensitivity analysis can be used to identify critical network components.

SSV analysis readily distinguishes the manifestations of uncertainties in global and local parameters, as well as identifies proteasome failure as a key fragility in apoptotic signaling. While the idea of labeling parameters based on their regulatory machinery has previously shown global parameters (transcriptional machinery, translational machinery, degradation machinery, etc.) to be more fragile and, therefore, necessitating more regulation, the character of the signaling network which is fragile is often unidentified. When perturbing individual interactions in the apoptotic network, local parameters are best suited for introducing delay/advance in the death signal, while global parameters readily affect the magnitude of the response. And while these results have strong experimental implications, SSV analysis provides a strong argument for system validation by identifying a known fragility in the Fas apoptotic network—namely, proteasome failure. The proteasome is the most important pathway controlling protein degradation (41) and is often targeted to indirectly influence apoptotic signaling (42). SSV analysis shows that minor perturbations in the degradation rates can easily amplify and nullify casp3 productions, a characteristic of the Fas signaling-induced apoptosis model which was not incorporated during parameter fitting. As more parameters in the network are measured, the case in Fig. 7 in which diffusion must maintain 25% uncertainty shows how SSV analysis can be used to further (in)validate the model.

Sensitivity analysis during apoptotic expression reveals that the death signal is robust to uncertainty in most interactions downstream of the apoptosome. SSV analysis could not be applied to the apoptotic response as linearizations about the upper steady state poorly captured signal dynamics. As stated, it is difficult to relate sensitivity to performance criteria, but in the case of apoptotic signaling, the only necessary performance metric after noise rejection is maintenance of the bistable behavior. Most of the parameters identified as sensitive during noise rejection remain sensitive during apoptosis response. The only downstream interaction to appear in the topmost sensitive parameters is the activation of casp3 via casp9. Inhibitor of apoptosis (IAP) is often targeted for regulating the death signal (43), but this appears to be a poor means to manipulate the network efficacy. But the best means of manipulating the apoptotic threshold and maintaining the bistable nature of the apoptotic network is by manipulating interactions upstream of the apoptosome.

Sensitivity analysis supports the claim that fragilities in apoptotic signaling are the result of system topology and not parameter tuning. Sensitivity analysis is a local measure, and, as such, it was calculated over several parameter sets to establish a more global measurement. Analyzing the distributions of the sensitivities for the global and local parameters in Fig. 8, the global parameters have a log normal distribution while the local parameter distributions are multimodal. Rankings for the global and local parameters when comparing the apoptotic and nonapoptotic sets show little variation, but for local parameters which show significant shifts in their mean sensitivity, it may be hypothesized that the sensitivity of the parameter is shifting between high and low nodes within the local distributions. These parameters were further scrutinized, revealing that while their means are statistically different when comparing their apoptotic and non-apoptotic distributions, the difference between their means is small. At most, parameter sensitivities shift from the low to middle mode of the distribution. Thus, the sensitivity distributions and their ensuing rankings are well maintained over all generated parameter sets, and parameter sensitivity of the apoptotic network is a characteristic of the network architecture and depends less on the fine tuning of parameters. And while feedback within this network is not significant in regulating the apoptotic response, feedforward regulation is a critical but robust feature of the network architecture.

In conclusion, robust performance analysis of the Fas apoptosis system supports topology as maintaining network performance, and identifies a known fragility, proteasomal failure. Given the simultaneous, allowable variation of parameter subsets are not overly restricted, it would appear that network topography is allowing for robust apoptotic performance, but, unlike other biochemical systems, this characteristic is not wholly maintained by integrated feedback regulation. Though Hill kinetics are, in themselves, a generalization of positive feedback, most of the signaling regulation is occurring upstream of the apoptosome formation. Robust performance analysis provides a powerful means of model (in)validation and model-based experimental design.

APPENDIX A

See Table 1 below.

TABLE 1

#	Parameter	Parameter value	Nonapoptotic rank*	Apoptotic rank†	P-value‡
1	GAPAF-1	3×10^{-4} μM/s	3.81	3.84	1.04×10^{-01}
2	GIAP	3×10^{-5} μM/s	35.46	30.26	8.39×10^{-04}
3	GPRO3	3×10^{-4} μM/s	27.78	19.22	6.99×10^{-03}
4	GPRO9	3×10^{-4} μM/s	20.66	9.18	1.11×10^{-02}
5	GBID	3×10^{-5} μM/s	16.21	17.78	1.03×10^{-01}
6	GBCL-2	9.5×10^{-6} μM/s	40.84	43.88	1.23×10^{-01}
7	GBAX	5.6×10^{-5} μM/s	1.89	3.91	1.24×10^{-01}
8	GCYT_MIT	3×10^{-4} μM/s	2.72	2.12	9.49×10^{-02}
9	μBAX	6×10^{-3} s^{-1}	14.31	14.83	1.07×10^{-01}
10	μAPAF-1	6×10^{-3} s^{-1}	7.85	7.69	1.04×10^{-01}
11	μIAP	6×10^{-3} s^{-1}	36.51	35.78	3.52×10^{-03}
12	μPRO3	6×10^{-3} s^{-1}	31.23	23.25	1.09×10^{-02}
13	μPRO9	6×10^{-3} s^{-1}	23.04	16.69	4.23×10^{-02}
14	μBID	6×10^{-3} s^{-1}	17.63	19.78	9.69×10^{-02}
15	μBCL-2	6×10^{-3} s^{-1}	48.78	48.57	1.91×10^{-01}
16	μCYTMIT	6×10^{-3} s^{-1}	12.04	11.61	1.14×10^{-01}
17	μCASP3	6×10^{-3} s^{-1}	26.37	30.29	7.76×10^{-01}
18	μCASP9	6×10^{-3} s^{-1}	28.73	32.83	8.10×10^{-01}
19	μTBID	6×10^{-3} s^{-1}	50.80	51.95	1.91×10^{-01}
20	μTBID BAX	6×10^{-3} s^{-1}	19.86	26.94	1.92×10^{-01}
21	μBAX_2	6×10^{-3} s^{-1}	9.92	12.74	1.69×10^{-01}
22	μTBIDMITO	6×10^{-3} s^{-1}	19.15	26.40	2.06×10^{-01}
23	μCYTC	6×10^{-3} s^{-1}	10.16	10.32	1.24×10^{-01}
24	μCASP8	6×10^{-3} s^{-1}	8.52	15.36	3.86×10^{-01}
25	k_{0p}	10 μM^{-1} s^{-1}	12.65	17.65	3.67×10^{-01}
26	k_{0m}	0.5 s^{-1}	14.85	21.25	3.67×10^{-01}
27	k_{0f}	0.1 s^{-1}	15.98	22.29	3.65×10^{-01}
28	k_{1p}	5 μM^{-1} s^{-1}	4.82	5.26	1.11×10^{-01}
29	k_{1m}	0.5 s^{-1}	5.82	6.31	1.11×10^{-01}
30	k_{1pb}	5×10^4 μM^{-1} s^{-1}	32.59	34.29	8.49×10^{-02}
31	k_{1mb}	0.5 s^{-1}	32.71	35.57	8.94×10^{-02}
32	k_{2p}	10 $\mu M^{-1} s^{-1}$	30.94	30.49	5.76×10^{-02}
33	k_{2m}	0.5 s^{-1}	36.73	35.90	5.58×10^{-02}
34	k_{3p}	10 μM^{-1} s^{-1}	35.72	33.38	4.11×10^{-02}
35	k_{3m}	0.5 s^{-1}	39.39	38.95	4.19×10^{-02}
36	k_{3f}	0.1 s^{-1}	38.36	36.96	3.28×10^{-02}
37	k_{4p}	5 μM^{-1} s^{-1}	52.88	53.23	2.31×10^{-04}
38	k_{4m}	0.5 s^{-1}	65.00	65.00	$0.00 \times 10^{+00}$
39	k_{4pb}	5 μM^{-1} s^{-1}	56.80	53.74	$0.00 \times 10^{+00}$
40	k_{4mb}	0.5 s^{-1}	64.00	63.83	$0.00 \times 10^{+00}$
41	k_{5p}	5 μM^{-1} s^{-1}	45.70	46.53	1.52×10^{-02}
42	k_{5m}	0.0035 s^{-1}	44.89	47.60	2.12×10^{-01}
43	k_{5pb}	5 μM^{-1} s^{-1}	58.34	55.81	1.00×10^{-15}
44	k_{5mb}	0.0035 s^{-1}	58.87	57.68	2.00×10^{-14}
45	k_{5pc}	5 μM^{-1} s^{-1}	56.11	54.89	4.46×10^{-12}
46	k_{5mc}	0.0035 s^{-1}	56.85	57.60	1.09×10^{-09}
47	k_{6p}	10 μM^{-1} s^{-1}	28.87	21.26	1.11×10^{-02}
48	k_{6m}	0.5 s^{-1}	29.93	22.47	1.14×10^{-02}
49	k_{6f}	0.001 s^{-1}	29.96	17.71	4.44×10^{-03}
50	k_{6I}	10 μM^{-1} s^{-1}	61.39	60.21	$0.00 \times 10^{+00}$
51	k_{6mb}	0.5 s^{-1}	62.39	61.28	$0.00 \times 10^{+00}$
52	k_{6fb}	0.1 s^{-1}	52.12	51.25	2.96×10^{-07}
53	k_{7p}	5 μM^{-1} s^{-1}	44.19	42.56	1.03×10^{-03}
54	k_{7m}	0.0035 s^{-1}	43.18	45.25	2.68×10^{-02}
55	k_{8p}	10 μM^{-1} s^{-1}	41.81	36.97	1.00×10^{-02}
56	k_{8m}	0.5 s^{-1}	44.44	41.65	9.86×10^{-03}
57	k_{8f}	0.1 s^{-1}	44.76	40.45	9.02×10^{-03}
58	k_{9p}	10 μM^{-1} s^{-1}	55.50	59.69	$0.00 \times 10^{+00}$
59	k_{9m}	0.5 s^{-1}	56.81	61.71	$0.00 \times 10^{+00}$
60	k_{9f}	0.1 s^{-1}	61.94	61.92	$0.00 \times 10^{+00}$

(*Continued*)

TABLE 1 (*Continued*)

#	Parameter	Parameter value	Nonapoptotic rank*	Apoptotic rank†	P-value‡
61	k_{11}	10 s^{-1}	10.84	21.54	4.88×10^{-01}
62	k_{12a}	10 μM^{-1} s^{-1}	22.59	25.74	1.42×10^{-01}
63	k_{12b}	10 μM^{-1} s^{-1}	22.44	25.26	1.33×10^{-01}
64	k_{13}	10 μM^{-1} s^{-1}	49.80	49.58	1.52×10^{-01}
65	k_{14}	10 μM^{-1} s^{-1}	7.80	9.04	1.29×10^{-01}

*Parameter sets for which 1×10^{-4} μM initial casp8 does not induce apoptosis are ranked based on their normalized sensitivity. Mean rankings are reported.
†Parameter sets for which 1×10^{-4} μM initial casp8 induces apoptosis are ranked based on their normalized sensitivity. Mean rankings are reported.
‡The p-value comparing the mean normalized sensitivity values of the apoptotic and nonapoptotic cases is calculated. The difference in the means is considered significant if the p-value is 0.05 or less.

APPENDIX B

Structured singular value (SSV) analysis is used to determine whether a system with bounded, properly distributed uncertainties can maintain stability and can provides a simple stability margin. One main advantage of SSV analysis over step and pulse response analyses is SSV analysis is done in the frequency domain and, as such, is well suited to characterize feedback stability. While many methods exist for determining stability in the frequency domain (Bode diagrams, etc.), Nyquist stability criterion is the basis for SSV analysis. A Nyquist plot is created simply by plotting real versus the imaginary component of the frequency response over all frequencies. Nyquist stability criterion states that for any open-loop system, G_{ol}, with P poles on the right of the imaginary axis (equivalent to the number of unstable eigenvalues), the system is stable under negative feedback as long as the Nyquist plot encircles $(-1,0)$ precisely P times. Fig. 11 provides an example application of Nyquist stability criterion (21). The open loop system, G_{OL} has one unstable eigenvalue and must encircle the $(-1,0)$ once to ensure stability under negative feedback. A gain (K) of 0.5 is insufficient to stabilize the system, but, by increasing the gain to 1.5, stability can be ensured.

The concept for robust stability (RS) via SSV analysis is an extension of the Nyquist stability criterion. Considering Fig. 11 further, allow the open loop transfer function to be stable and allow some uncertainty in the gain of the negative feedback such that $K \in [k_{low}, k_{high}]$. Starting with a stable, nominal system G_{OL} ($P = 0$), RS is guaranteed so long as the Nyquist plots for all possible values of the perturbation between k_{low} and k_{high} do not encircle the critical point $(-1,0)$. Now one needs only a method to determine the size of the perturbation which destabilizes the feedback system.

The first step to applying SSV analysis is the proper construction of the uncertainty system. The structure of the uncertainty comes from applying uncertainty perturbations to specific interactions within the network. Fig. 12 illustrates how a nominal system with uncertainty about two of the internal transfer functions is shaped into the $P\Delta$ block in which the uncertainties are lumped into the Δ block. The uncertainties are designed to be of size 1 ($\|\delta_i\|$ inf $\leq$ 1), and the weighting blocks (W_1 and W_1) are used to tune the magnitude of the uncertainty. Once in the $P\Delta$ block structure, it is easy to reshape the system to the $M\Delta$ block via a linear fractional transformation. Stability is independent of the magnitude of the input for a linear system (as seen in the $M\Delta$ block), and generally for uncertainty analysis, the nominal system is stable. Thus, Nyquist stability criterion is applied to the $M\Delta$ block system.

The precise definition of μ for RS of the $M\Delta$ block is

$$\mu(\mathbf{M})^{-1} \triangleq \min_{\Delta}\{\bar{\sigma}(\Delta)|\det(\mathbf{I} - \mathbf{M}\Delta) = \mathbf{0} \text{ for structured } \Delta\}. \tag{4}$$

Under positive feedback and by subtracting the open-loop system from an identity matrix, the critical point for Nyquist criterion shifts to the origin. Thus, when the det($\mathbf{I - M\Delta}$) crosses zero, it is equivalent to one of the stable eigenvalues crossing the imaginary axis. If $\mathbf{\Delta}$ is >1 ($\mu < 1$), then system uncertainty must exceed the predefined limits to force instability and the system is RS. Calculating μ is an NP hard problem and considerable literature exists on the topic (21,24,25). A precise value of μ is generally not available for larger systems, and, instead, the value of $\mu(\mathbf{M})$ is bounded above by the maximum singular value of $\mathbf{M}$ and below by the spectral radius of $\mathbf{M}$. This analysis can be extended to robust performance (RP) by closing the input/output channels with an unstructured uncertainty block (full block matrix with a norm of 1). In doing so, one is restricting the ratio of the input/output channels to <1, and μ measures the amount of uncertainty required to push the system to the performance bounds.

This work was supported by the Institute for Collaborative Biotechnologies through grant No. DAAD19-03-D-0004 from the U.S. Army Research Office, Integrative Graduate Education and Research Traineeship National Science Foundation grant No. DGE02-21715, and the University of California, Board of Regents.

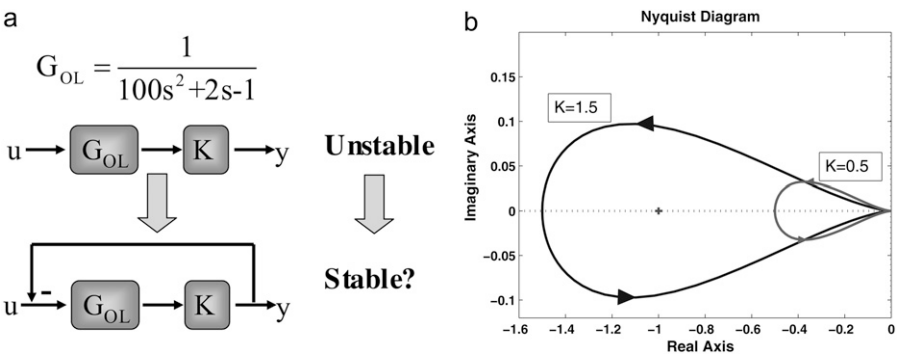

FIGURE 11 Application of the Nyquist stability criterion. For an example of open-loop transfer function, G_{OL}, with one stable pole at -0.11 and one unstable pole at 0.09, the Nyquist plot must encircle $(-1,0)$ exactly once to have stability under negative feedback. When the gain, K, is set to 0.5, the closed-loop system remains unstable, but the system is stabilized under negative feedback when the gain is increased to 1.5.

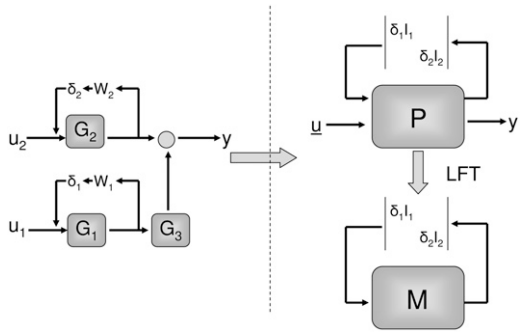

FIGURE 12 An example of an uncertain system that is shaped into the PΔ block system, where Δ is the block-diagonal matrix, $[\delta_1 I_1\ \delta_2 I_2]$. This system can be lifted via linear fractional transformation to the $M\Delta$ block structure and tested for robust stability. Closing the input/output channels of the $P\Delta$ block structure, one can test for robust performance.

REFERENCES

1. Parrino, J., and B. S. Graham. 2006. Smallpox vaccines: past, present, and future. *J. Allergy Clin. Immunol.* 118:1320–1326.
2. Wang, M. D., D. M. Shin, J. W. Simons, and S. Nie. 2007. Nanotechnology for targeted cancer therapy. *Expert Rev. Anticancer Ther.* 7:833–837.
3. Linehan, W. M., P. A. Pinto, R. Srinivasan, M. Merino, P. Choyke, L. Choyke, J. Coleman, J. Toro, G. Glenn, C. Vocke, B. Zbar, L. S. Schmidt, D. Bottaro, and L. Neckers. 2007. Identification of the genes for kidney cancer: opportunity for disease-specific targeted therapeutics. *Clin. Cancer Res.* 13:671s–679s.
4. Zhong, S., A. T. Macias, and A. D. MacKerell. 2007. Computational identification of inhibitors of protein-protein interactions. *Curr. Top. Med. Chem.* 7:63–82.
5. McAdams, H. H., and A. Arkin. 1999. It's a noisy business! Genetic regulation at the nanomolar scale. *Trends Genet.* 15:65–69.
6. Stelling, J., U. Sauer, Z. Szallasi, F. J. Doyle III, and J. Doyle. 2004. Robustness of cellular functions. *Cell.* 118:675–685.
7. Kitano, H. 2002. Systems biology: a brief overview. *Proc. Natl. Acad. Sci. USA.* 295:1662–1664.
8. Meier, P., A. Finch, and G. Evan. 2000. Apoptosis in development. *Nature.* 407:796–801.
9. Screpanti, V., R. P. A. Wallin, A. Grandien, and H. Ljunggren. 2005. Impact of FASL-induced apoptosis in the elimination of tumor cells by NK cells. *Mol. Immunol.* 42:495–499.
10. Matter, C. M., C. E. Chadjichristos, P. Meier, T. von Lukowicz, C. Lohmann, P. K. Schuler, D. Zhang, B. Odermatt, E. Hofmann, T. Brunner, B. R. Kwak, and T. F. Lüscher. 2006. Role of endogenous Fas (CD95/Apo-1) ligand in balloon-induced apoptosis, inflammation, and neointima formation. *Circulation.* 113:1879–1887.
11. Krammer, P. H. 2000. CD95's deadly mission in the immune system. *Nature.* 407:789–795.
12. Barkai, N., and S. Leibler. 1997. Robustness in simple biochemical networks. *Nature.* 387:913–917.
13. Bagheri, N., J. Stelling, and F. J. Doyle. 2007. Quantitative performance metrics for robustness in circadian rhythms. *Bioinformatics.* 23:358–364.
14. Stelling, J., E. D. Gilles, and F. J. Doyle III. 2004. Robustness properties of circadian clock architectures. *Proc. Natl. Acad. Sci. USA.* 101:13210–13215.
15. Eissing, T., F. Allgöwer, and E. Bullinger. 2005. Robustness properties of apoptosis models with respect to parameter variations and intrinsic noise. *Syst. Biol. (Stevenage).* 152:221–228.
16. Schmidt, H., and E. W. Jacobsen. 2004. Linear systems approach to analysis of complex dynamic behaviors in biochemical networks. *IEE Sys. Biol.* 1:149–158.
17. Varma, A., M. Morbidelli, and H. Wu. 1999. Parametric Sensitivity in Chemical Systems. Oxford University Press, New York, NY.
18. Yetter, R., F. Dryer, and H. Rabitz. 1985. Some interpretive aspects of elementary sensitivity gradients in combustion kinetics modeling. *Combust. Flame.* 59:107.
19. Kikuchi, S., K. Fujimoto, N. Kitagawa, T. Fuchikawa, M. Abe, K. Oka, K. Takei, and M. Tomita. 2003. Kinetic simulation of signal transduction system in hippocampal long-term potentiation with dynamic modeling of protein phosphatase 2A. *Neural Netw.* 16:1389–1398.
20. Taylor, S. R., K. Gadkar, R. Gunawan, and F. J. Doyle III. 2004. BioSens: a sensitivity analysis toolkit for Bio-SPICE. http://doyle.chemengr.ucsb.edu.
21. Skogestad, S., and I. Postlethwaite. 1996. Multivariable Feedback Control. Analysis and Design. Wiley, Chichester, UK.
22. Skogestad, S., M. Morari, and J. C. Doyle. 1988. Robust control of ill-conditioned plants: high-purity distillation. *IEEE Trans. Automat. Contr.* 33:1092–1105.
23. Paduano, J., and D. Downing. 1984. Sensitivity analysis of digital flight control systems using singular-value concepts. *J. Guid. Control Dyn.* 12:297.
24. Braatz, R. P., P. M. Young, J. C. Doyle, and M. Morari. 1994. Computational-complexity of μ calculation. *IEEE Trans. Automat. Contr.* 39:1000–1002.
25. Doyle, J. C., B. A. Francis, and A. R. Tannenbaum. 1992. Feedback Control Theory. Macmillan Publishing Company, New York.
26. Ferreres, G., and V. Fromion. 1997. Computation of the robustness margin with the skewed μtool. *Syst. Contr. Lett.* 32:193–202.
27. Elojeimy, S., J. C. McKillop, A. M. El-Zawahry, D. H. Holman, X. Liu, D. A. Schwartz, T. A. Day, J.-Y. Dong, and J. S. Norris. 2006. FasL gene therapy: a new therapeutic modality for head and neck cancer. *Cancer Gene. Ther.* 13:739–745.
28. Bentele, M., I. Lavrik, M. Ulrich, S. Stösser, D. W. Heermann, H. Kalthoff, P. H. Krammer, and R. Eils. 2004. Mathematical modeling reveals threshold mechanism in CD95-induced apoptosis. *J. Cell Biol.* 166:839–851.
29. Fussenegger, M., J. E. Bailey, and J. Varner. 2000. A mathematical model of caspase function in apoptosis. *Nat. Biotechnol.* 18:768–774.
30. Hua, F., M. G. Cornejo, M. H. Cardone, C. L. Stokes, and D. A. Lauffenburger. 2005. Effects of Bcl-2 levels on Fas signaling-induced caspase-3 activation: molecular genetic tests of computational model predictions. *J. Immunol.* 175:985–995.
31. Hua, F., S. Hautaniemi, R. Yokoo, and D. A. Lauffenburger. 2006. Integrated mechanistic and data-driven modeling for multivariate analysis of signaling pathways. *J. R. Soc. Interface.* 3:515–526.
32. Bagci, E. Z., Y. Vodovotz, T. R. Billiar, G. B. Ermentrout, and I. Bahar. 2006. Bistability in apoptosis: roles of bax, bcl-2, and mitochondrial permeability transition pores. *Biophys. J.* 90:1546–1559.
33. Nair, V. D., T. Yuen, C. W. Olanow, and S. C. Sealfon. 2004. Early single cell bifurcation of pro- and antiapoptotic states during oxidative stress. *J. Biol. Chem.* 279:27494–27501.
34. Ishioka, T., R. Katayama, R. Kikuchi, M. Nishimoto, S. Takada, R. Takada, S. i. Matsuzawa, J. C. Reed, T. Tsuruo, and M. Naito. 2007. Impairment of the ubiquitin-proteasome system by cellular FLIP. *Genes Cells.* 12:735–744.
35. Fu, N. Y., S. K. Sukumaran, and V. C. Yu. 2007. Inhibition of ubiquitin-mediated degradation of MOAP-1 by apoptotic stimuli promotes Bax function in mitochondria. *Proc. Natl. Acad. Sci. USA.* 104:10051–10056.
36. Kim, S., K. Choi, D. Kwon, E. N. Benveniste, and C. Choi. 2004. Ubiquitin-proteasome pathway as a primary defender against TRAIL-mediated cell death. *Cell. Mol. Life Sci.* 61:1075–1081.
37. Karpinich, N. O., M. Tafani, R. J. Rothman, M. A. Russo, and J. L. Farber. 2002. The course of etoposide-induced apoptosis from damage

to DNA and p53 activation to mitochondrial release of cytochrome *c*. *J. Biol. Chem.* 277:16547–16552.

38. Adamkova, L., K. Souckova, and J. Kovark. 2007. Transcription protein STAT1: biology and relation to cancer. *Folia Biol. (Praha).* 53:1–6.
39. Kurdi, M., and G. W. Booz. 2007. Jak inhibition, but not Stat1 knockdown, blocks the synergistic effect of IFN-γ on Fas-induced apoptosis of A549 human non-small cell lung cancer cells. *J. Interferon Cytokine Res.* 27:23–31.
40. Choi, H.-S., S. Han, H. Yokota, and K.-H. Cho. 2007. Coupled positive feedbacks provoke slow induction plus fast switching in apoptosis. *FEBS Lett.* 581:2684–2690.
41. Galimberti, S., M. Canestraro, S. Pacini, R. Fazzi, E. Orciuolo, L. Trombi, L. Mattii, B. Battolla, A. Capodanno, P. Collecchi, F. Veroni, P. Simi, S. Piaggi, A. Casini, and M. Petrini. 2007. PS-341 (Bortezomib) inhibits proliferation and induces apoptosis of megakaryoblastic MO7-e cells. *Leuk Res.* In press.
42. Voortman, J., T. P. Resende, M. A. I. A. E. Hassan, G. Giaccone, and F. A. E. Kruyt. 2007. TRAIL therapy in non-small cell lung cancer cells: sensitization to death receptor-mediated apoptosis by proteasome inhibitor Bortezomib. *Mol. Cancer Ther.* 6:2103–2112.
43. Zhang, H.-G., J. Wang, X. Yang, H.-C. Hsu, and J. D. Mountz. 2004. Regulation of apoptosis proteins in cancer cells by ubiquitin. *Oncogene.* 23:2009–2015.